TECHNICAL PAPER

Efficacy of External Stationary Shoulder for Controlling Residual Stress and Distortion in Friction Stir Welding

Weiliang He[1] · **Mingshen Li**[1] · **Qi Song**[1] · **Jinglin Liu**[1] · **Wei Hu**[1]

Abstract Considerable residual stress and distortion are inevitably produced by friction stir welding (FSW). An external stationary shoulder was applied to control and eliminate the residual stress and distortion of FSW joint. A thermo-mechanical model was utilized to analyze the effects of rotational velocities on temperature and stress distribution during welding. Results showed that the stationary shoulder provided synchronous rolling and intense cooling functions during welding, which reduced the peak residual tensile stress near the weld of FSW. The residual distortion of FSW joint was greatly reduced by the external stationary shoulder.

Keywords Friction stir welding · Stationary shoulder · 2024-T4 aluminum alloy · Residual stress · Synchronous rolling · Distortion

1 Introduction

Aluminum alloys have been widely used in the field of manufacturing due to their excellent extrusion formability, high corrosion resistance and good weldability [1]. Currently, the welding techniques for aluminum alloys, such as fusion welding and friction stir welding (FSW), have attracted significant attention of related researchers [2]. FSW, which is a solid-state joining method, was invented by Wayne Thomas at The Welding Institute (TWI) in 1991 [3, 4]. FSW can avoid common defects in fusion welding, such as insufficient fusion and hot cracking [5, 6]. Thus, FSW has gradually become an effective method of aluminum alloy welding and has been widely applied to relevant industrial fields. However, welding residual stress and distortion are inevitable in FSW, which are caused by the existence of welding thermal input and its non-uniform distribution [7]. Long et al. [8] and Riahi et al. [9] indicated that significant residual stress and distortion were generated despite the low temperature solid-state nature of FSW when the peak welding temperature approached melting point of material. The existence of residual stress affects the structure service performance by inducing early fatigue failure and stress corrosion cracking [10].

To date, several researchers have investigated the methods to reduce residual stress and distortion of FSW. Tufaro et al. [11] reduced the temperature gradient by optimizing the welding parameters and obtained a relatively low residual stress in AA7075-T651 FSW joint. Ji et al. [12] found that the trailing intensive cooling was beneficial in reducing the peak temperature during FSW and decreasing the welding distortion. The reduction of thermal input had a positive effect on decreasing residual stress and distortion of FSW. However, the excessively low welding thermal input may lead to a series of defects, such as grooves and cavities [13]. In addition, some non-thermal factors have also been studied. Richter-Trummer et al. [14] found that higher clamping force led to a lower distortion and a more uniform residual stress distribution through the thickness. However, FSW residual stress and distortion could not be significantly controlled by only reducing the peak temperature or applying high clamping force.

According to the above-mentioned researches, finding a new method to reduce the residual stress and distortion of

---

Weiliang He and Mingshen Li contributed equally to this work.

✉ Qi Song
songqi201806@126.com

1 School of Aerospace Engineering, Shenyang Aerospace University, Shenyang 110136, People's Republic of China

FSW has become the focus of research. A technology named stationary shoulder friction stir welding (SSFSW) can be considered for controlling residual stress and distortion. SSFSW was developed by TWI in 2004, which was initially designed to improve the uneven distribution of welding heat along the thickness of the Ti–6Al–4V titanium alloy [15, 16]. During SSFSW process, an inside rotating tool provides the welding heat through its friction with material, and an outside non-rotating shoulder compresses the material and slides on the plate surface [17].

Currently, few researchers have investigated the welding stress and distortion in SSFSW. Sun et al. [18] investigated the effect of welding speed on residual stress of 6.3-mm-thick AA7010 aluminum alloy plate by SSFSW. They found that with the increase in welding speed, the peak residual tensile stress increased but the distribution region of the residual tensile stress narrowed. Up till now, few studies have focused on the reduction of welding residual stress and distortion of thin aluminum alloy plate by SSFSW, these topics need to be further studied [19, 20]. In this study, the influences of rotational velocities on residual stresses and distortions of thin 2024-T4 aluminum alloy plates under FSW and SSFSW processes were investigated by numerical and experimental methods.

2 Experimental Produce

In this study, 2024-T4 aluminum alloy (Al 2024-T4) plate with dimensions of 200 mm × 90 mm × 3 mm was utilized as base metal. The chemical compositions of Al 2024-T4 are given in Table 1. A tool consisting of a six-helix concave shoulder with diameter of 10 mm and a conical threaded pin with length of 2.7 mm was used in the experiment, and the diameters of the root and tip of the pin were 4.5 and 3.5 mm, respectively. Before welding, all plates were polished by different grades of emery paper to wipe off the oxidation layer. During the conventional FSW and SSFSW processes, a tool tilt angle of 2.5° was used.

The schematic of the SSFSW welding process and detailed descriptions of the welding tool are shown in Fig. 1. The tool was rotated along the weld line in anti-clockwise direction; so the advancing side (AS) and retreating side (RS) were located on the left and right of the
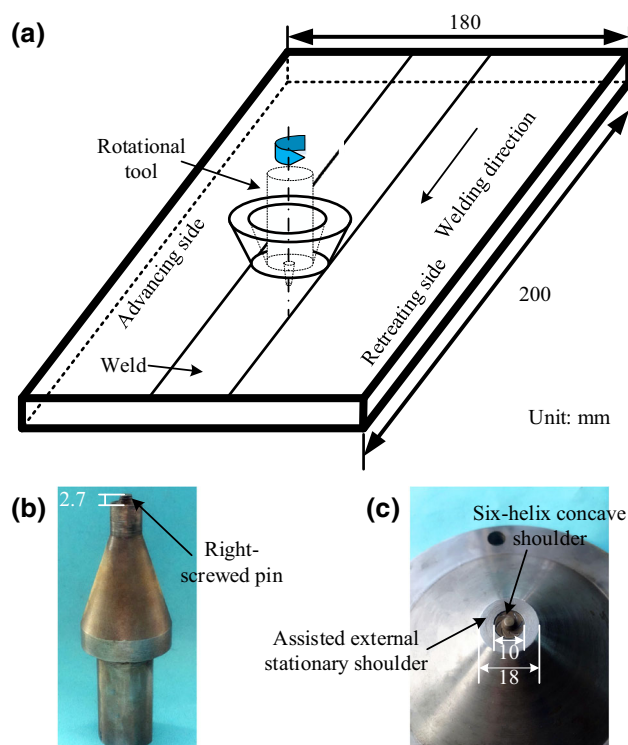

Fig. 1 **a** Schematic of the SSFSW; images of **b** rotational tool and **c** stationary shoulder used in experiment

welding line, respectively. The welding parameters directly affected the distribution of temperature and residual stress, and the appropriate selection of parameter was premised on the basis of avoidance of defect in the stir zone (SZ). Wang et al. [21] investigated the distributions of temperature and residual stress with Al 2024 and found that the peak stress in the longitudinal directions was mainly influenced by the rotational velocity rather than welding speed. In addition, Cao et al. [22] further indicated that the low temperature resulted in the formation of discontinuity and ultimately initiated voids. According to these previous reports, this study mainly focused on the effect of rotational velocity on the residual stress. The welding parameters of conventional and stationary shoulders are displayed in Table 2. The welding speed had a constant value of 150 mm/min, and the rotational velocity varied from 800 rpm to 1200 rpm. Figure 2 exhibits the smooth surface appearances of the FSW joints by using the assisted external stationary

Table 1 Chemical compositions of 2024-T4 aluminum alloy (wt%)

Weight%	Si	Fe	Cu	Mn	Mg	Zn	Ni	Cr	Al
Minimum	–	–	3.5	–	0.09	–	1.7	–	90.5
Maximum	0.7	1.0	4.5	0.2	0.45	0.25	2.3	0.1	94.71

Table 2 Conventional FSW and SSFSW welding parameters used in this study

No.	Designation	Rotational velocity (rpm)	Welding speed (mm/min)
1	F800/150	800	150
2	F1000/150	1000	
3	F1200/150	1200	
4	SS800/150	800	
5	SS1000/150	1000	
6	SS1200/150	1200	
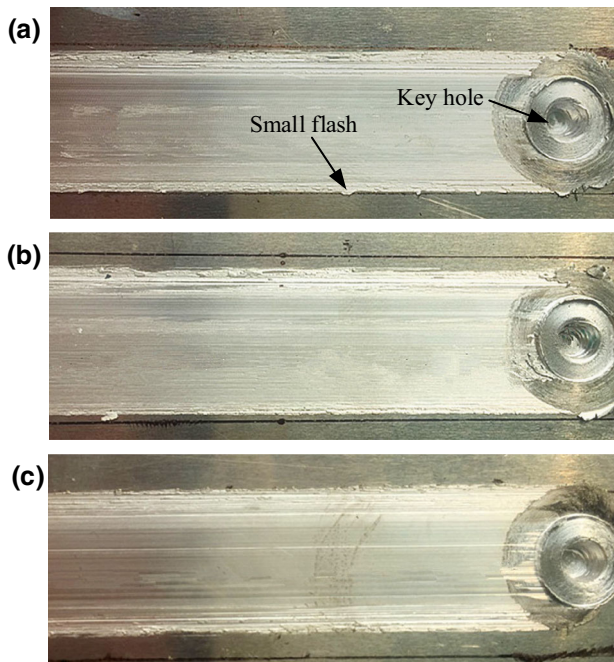
Fig. 2 Surface appearances of FSW joints assisted by external stationary shoulder at **a** 800 rpm, **b** 1000 rpm and **c** 1200 rpm

shoulder, which partly verified the rationality of the selection of rotational velocity because no groove defect was observed.

Temperature histories of the observation points were recorded by K-type thermocouples. The schematic diagram of thermocouple positions and the dimension of metallographic specimen are shown in Fig. 3. The thermocouple was inserted into a 1.5 mm diameter hole with a depth of 0.5 mm away from the top surface of the plate. After welding, metallographic specimens were cut perpendicular to the welding direction by an electrical discharge cutting machine. In order to analyze the influence of rotational velocities on the microstructures in each area, such as the SZ and the shoulder affected zone, Keller reagent was used to etch the metallographic specimens and an optical microscope was used to observe the macrographs of weld cross-sections.

3 Model Description

The nonlinear temperature-dependent material properties of Al 2024-T4 were selected from Refs. [23, 24] and are shown in Fig. 4. Numerical simulations of welding processes were performed by using ABAQUS/standard FEM software. Two steps, namely a thermal transfer step to forecast the welding temperature field and a synchronous rolling step to modify the welding residual stress, were used to simulate the welding process. The employed step time period in the heat transfer model was 60 s along the 150 mm length of the plate. The moving velocity of the heat source was 150 mm/min (i.e., 2.5 mm/s).

3.1 Meshing

Currently, economy and accuracy are the significant factors used for numerical analysis. Therefore, the element type of C3D8T (an 8-node thermally coupled brick, trilinear displacement, and temperature) was utilized in this study. A typical mesh for Al 2024-T4 was employed, as shown in Fig. 5. The total number of elements was 61,200 elements. The mesh size near the weld was $1 \times 1 \times 1$ mm to ensure the computational accuracy, and the maximum size in the vertical weld direction was $4 \times 1 \times 1$ mm with a gradual increasing tendency.

3.2 Boundary Conditions

The thermal and mechanical boundary conditions for numerical simulation are shown in Fig. 6. In the simulation process, the backing plate and the pressing plates were used to mechanically constrain the welded plate. The heat losses through the backing plate or the pressing plates were considered. The contact conductivities between the welding plate and the backing plate or pressing plates were assumed to be 150 and 100 W/(m^2 °C), respectively. The free convection heat transfer coefficient between the plate and atmosphere was set as 20 W/(m^2 °C). The uniform thermal emissivity was set to 0.75, and the ambient temperature was presumed to a constant value of 20 °C. The external stationary shoulder synchronously absorbed a considerable amount of heat, which was considered as a variable heat conduction loss to the weld. Therefore, a temperature-dependent convection coefficient was applied between the weld and ambient temperature. The value was set as 35 W/(m^2 °C).

3.3 Thermal Model

In this model, the heat production of rotational shoulder and pin was considered. The welding heat source was

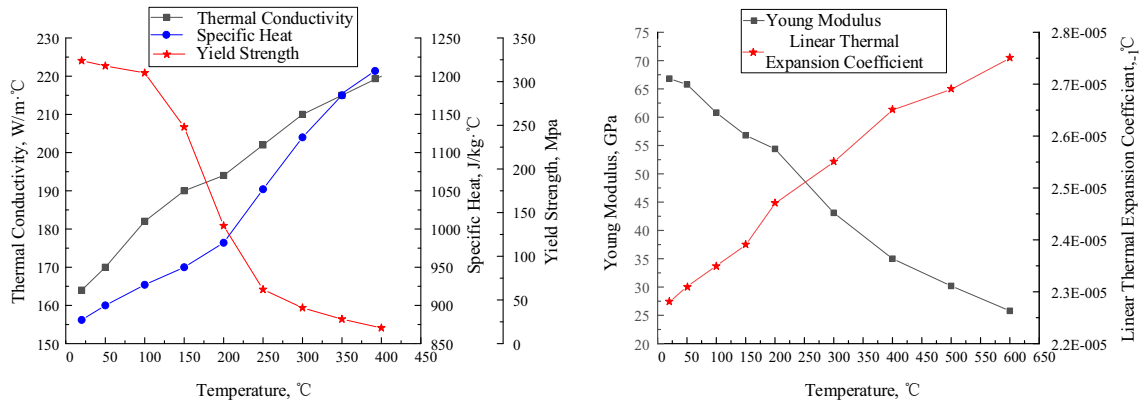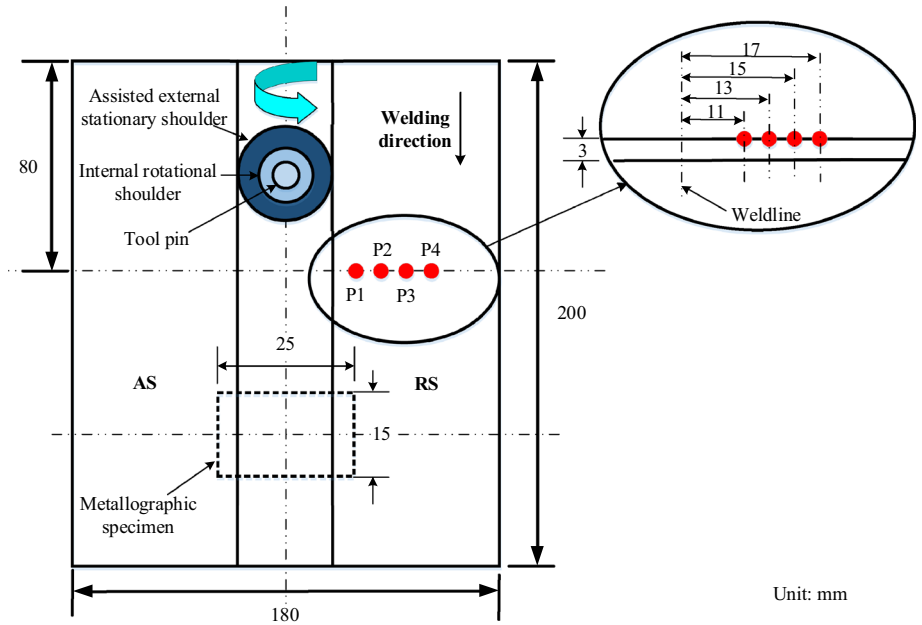**Fig. 3** Schematic diagram of thermocouple positions and metallographic specimen

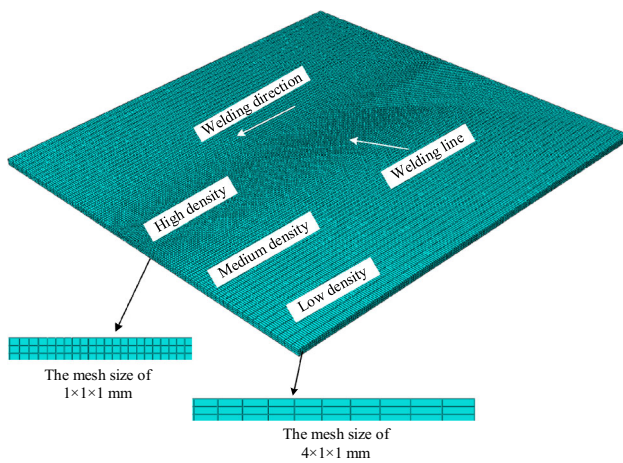**Fig. 4** Temperature-dependent material properties of Al 2024-T4

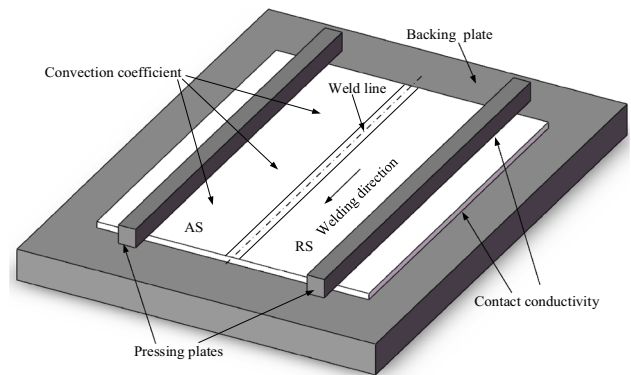**Fig. 5** Global view of different mesh densities

Fig. 6 Boundary conditions in simulation

considered from two aspects, one is the surface heat source produced by the friction between the shoulder and the plate, the other is the body heat source produced by the friction between the pin and the plate. The surface heat flux was calculated by Fourier's formulation as follows:

$$Q_s = \int_{r_0}^{R_0} 2\pi\mu wP \cdot r^2 \mathrm{d}r = \frac{2}{3}\pi\mu wP \cdot \left(R_0^3 - r_0^3\right) \qquad (1)$$

and

$$w = \frac{2\pi n}{60} \qquad (2)$$

and then the heat produced by shoulder can be expressed as:

$$Q_s = \frac{1}{45}\pi^2\mu nP \cdot \left(R_0^3 - r_0^3\right) \qquad (3)$$

where Q_s is the surface heat flux, R_0 is the shoulder radius ($R_0 = 5$ mm), r_0 is the average radius of pin ($r_0 = 2$ mm), μ is the frictional coefficient, w is the angular velocity of the tool, n is the rotational velocity of the tool, and P is the tool plunge pressure. The pressure of external stationary shoulder (7500 N) is larger than that of internal rotational shoulder (1500 N).

The heat produced by pin (Q_P) is expressed by [25]:

$$Q_p = \frac{1}{45}\pi^2\mu nP \cdot \left(r_0^3 + 3r_0^3 L_p\right) \qquad (4)$$

where L_p is the length of the pin. The two simplified thermal input equations [Eqs. (3) and (4)] ensured that rational thermal input was provided to the model.

The welding process could be divided into the heating and cooling stages. At the heating stage, severe localized heating induced the thermal gradient that generated thermal stresses and welding distortion. At the cooling stage, the temperature of the plate gradually dropped to ambient temperature, and several thermal stresses were still clasped in the pressing plates. To accurately capture the stress field evolution, an extra step named "step-unload" was added to simulate unclamping. In this step, the clamping restraint of the weld and its surrounding area were completely removed in all degrees of freedom after welding.

4 Results and Discussion

4.1 Comparison on Numerical and Experimental Results

Figure 7 shows the comparison between the simulated and experimentally measured temperatures developed in FSW and SSFSW. With the approaching and leaving of the welding heat source, the temperature of the observation

point increases rapidly and then decreases. The maximum relative error is approximately 2.37% for the conventional process, which is nearly 3.14% for the stationary shoulder process. The frictional coefficient, contact conductivity, and free convection coefficient are determined to have a significant influence on the errors of temperature histories. In this model, the frictional coefficients are set to 0.3 and 0.32 for FSW and SSFSW, respectively, and the contact conductivity and free convection coefficient are assumed as constant values to promote the numerical simulation. In the actual experiment, the contact conductivity and free convection coefficient vary with the change in the plate temperature. However, the figure shows an acceptable agreement between the numerical and experimental results and the accurate prediction of temperature history provides satisfactory results.

4.2 Analysis on Temperature Field and Weld Macrostructures

The temperature curves of different observation points along the thickness direction during conventional FSW and SSFSW are compared in Fig. 8. The thermal cycle shows relatively small temperature gradient between the upper and lower surfaces, because the thin plate has been used and its heat conduction is high. The thermal histories of weld center during conventional FSW and SSFSW processes under different rotational velocities are displayed in Fig. 9. The peak temperature of SSFSW is approximately 30 °C below that of conventional FSW under the same velocity. Different rotational velocities inevitably generate differences in material shearing and frictional forces, and the higher rotational velocities cause the larger thermal input and then the higher peak temperature. In addition, the heating rate at the heating stage of SSFSW is lower than conventional FSW, whereas the cooling rate at the cooling stage of SSFSW is higher than that of conventional FSW. This is because, a large quantity of frictional heat is absorbed by the non-rotating external stationary shoulder for SSFSW.

Figure 10 shows the macroview cross-sections of the produced conventional FSW and SSFSW joints with different rotational velocities. No defects (such as holes) are observed in the welded joints at rotational velocities from 800 to 1200 rpm, which further prove the reasonability of the selected welding parameters. A large flash (Fig. 10) is generated by the conventional FSW, which results in weld thickness reduction. For the SSFSW, the external stationary shoulder effectively prevents plasticized materials escaping from the SZ, and the flash is greatly reduced (Fig. 2). The cross section of SZ for the conventional FSW presents a bowl-like shape, and the SZ shape for the SSFSW is similar to the rotating pin. The widths of SZ are significantly
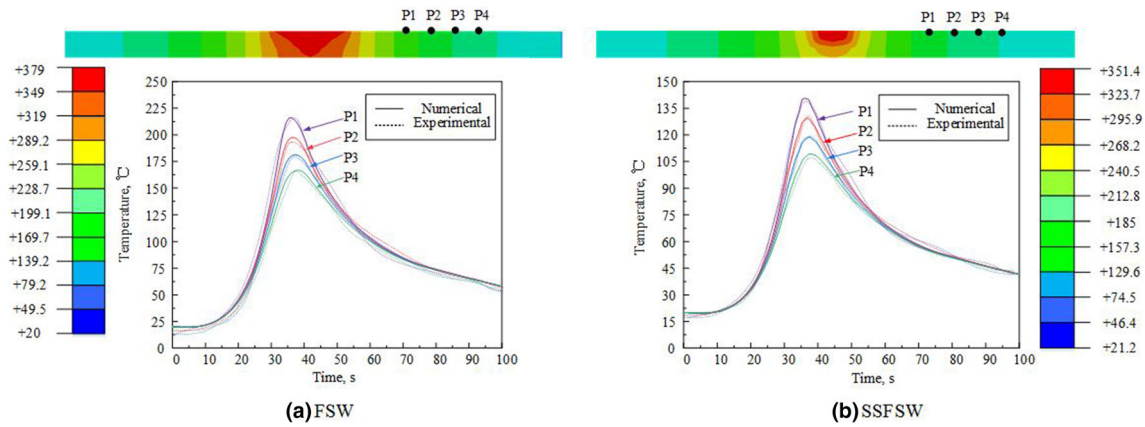
Fig. 7 Thermal cycle comparisons of experimental and numerical methods at 800 rpm by **a** FSW and **b** SSFSW
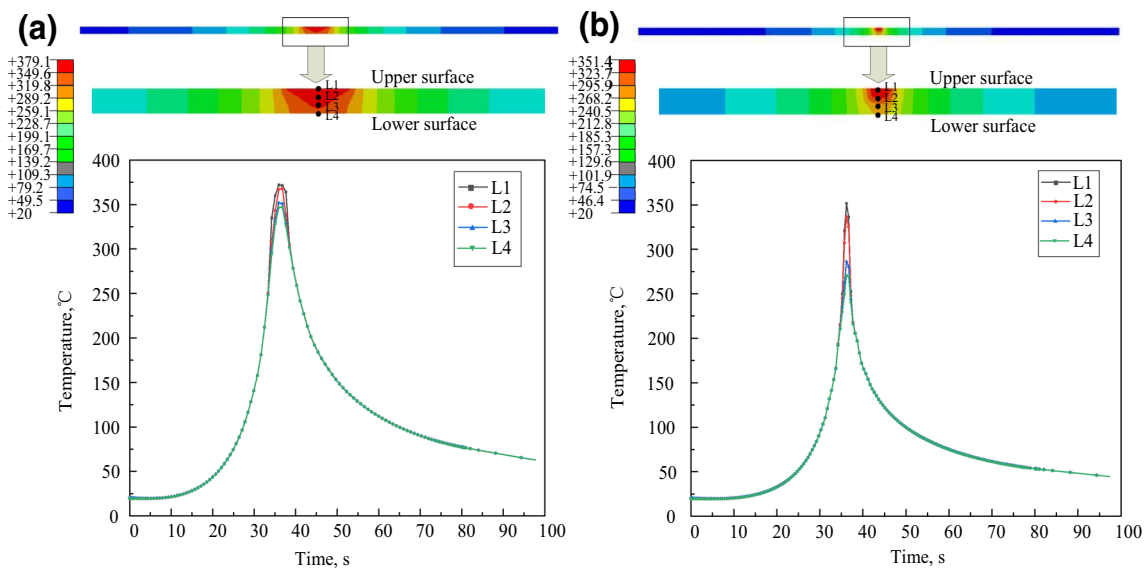

Fig. 8 Temperature histories of different positions along the thickness direction by simulation at 800 rpm under **a** conventional FSW and **b** SSFSW
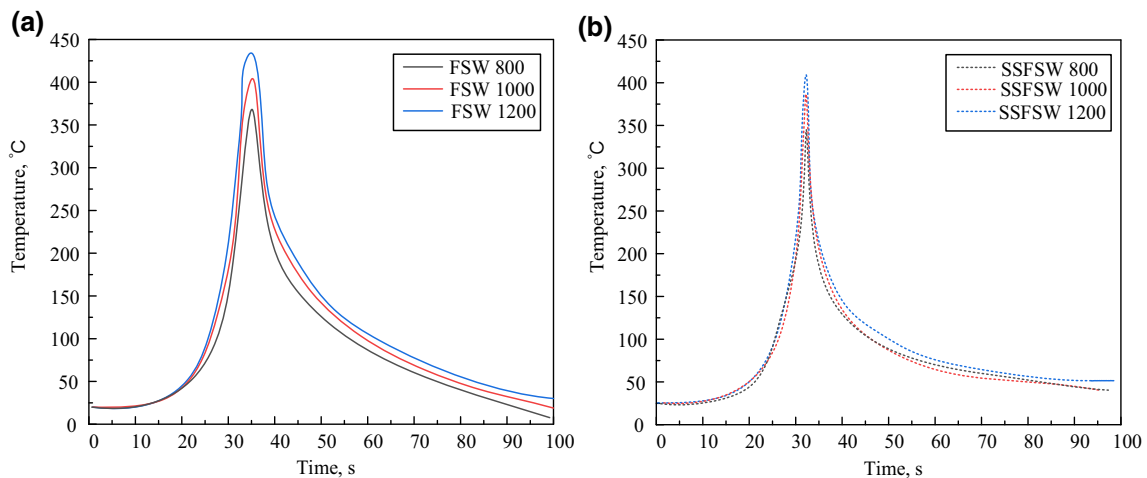

Fig. 9 Temperature histories of weld center under **a** conventional FSW and **b** SSFSW by numerical simulation
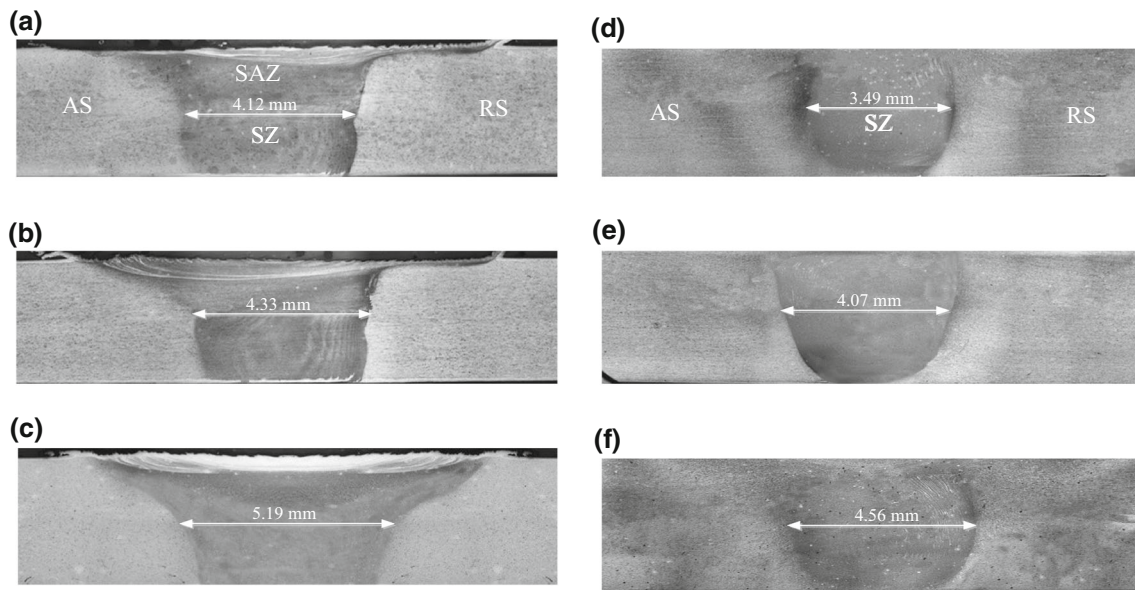
Fig. 10 Macroscopic appearances of welded joints by conventional FSW with rotational velocities of **a** 800 rpm, **b** 1000 rpm, **c** 1200 rpm and SSFSW with rotational velocities of **d** 800 rpm, **e** 1000 rpm, **f** 1200 rpm

influenced by the tool rotational velocity. A high thermal input and sufficient plastic material flow increases the width of SZ with the increase of tool rotational velocity. The non-rotating external stationary shoulder absorbs massive amounts of heat and ensures uniform temperature distribution in the thickness section. Thus, the widths of SZ produced by the conventional FSW are larger than that by the SSFSW. At the top surface, the concave shoulder has a significant effect on the microstructural profile for conventional FSW. The width of SAZ is approximately the same with the diameter of the rotational concave shoulder. However, the non-rotating external stationary shoulder provides intense cooling during welding. A portion of heat is absorbed by the stationary shoulder, and the frictional heat between the stationary shoulder and plate is nearly ignored. Thus, the width of SAZ is greatly reduced and is nearly the same value with the bottom diameter of the rotational pin for SSFSW.

4.3 Analysis on Stress and Distortion

This study focuses on the residual stress along the longitudinal welding direction. During welding, the longitudinal stress is associated with the peak temperature. The comparison of welding stress contours on the upper surface by conventional FSW and SSFSW is represented in Fig. 11. Three different regions of SSFSW process at 800 rpm rotational velocity are selected in Fig. 11b. Although the material under stationary shoulder suffers a stronger mechanical force and then produces a higher tensile stain, a compressive stress lower than that before the stationary

shoulder appears in the weld region in contact with the stationary shoulder (line 1 in Fig. 11b). This mainly results from the more serious material softening induced by the higher temperature. With the welding heat source moving away, the material in weld (line 2 in Fig. 11b) experiences a tensile strain, because the temperature of this material gradually decreases and the accompanied shrinkage is constrained by the materials on both sides of weld. Therefore, the tensile stress appears in the region behind the tool (line 2 in Fig. 11b). With further decrease of temperature in the weld behind the tool (line 3 in Fig. 11b), the tensile stress increases.

The longitudinal residual stress (LRS) distributions perpendicular to the weld with different rotational velocities are shown in Fig. 12. The LRS profile on the upper surface presents an "M" shape, and the peak value of tensile residual stress (TRS) is situated at the transition region between the heat-affected zone (HAZ) and SZ, which mainly results from the following three reasons. Firstly, the temperature near the weld is much higher, which easily produces higher tensile stress. Secondly, the inside rotational tool provides a large vertical force on the weld, which is beneficial to reduce the tensile stress. Finally, the reduced effect of tensile stress in the weld by the rotational tool gradually decreases with the increase in distance away from the weld line. The high rotational velocity produces a large quantity of frictional heat to the weld, resulting in the increase in peak TRS. The maximum TRS under conventional FSW at rotational velocities of 800, 1000 and 1200 rpm are 109.8, 123.1, and 132.7 MPa, respectively. The external assisted stationary shoulder
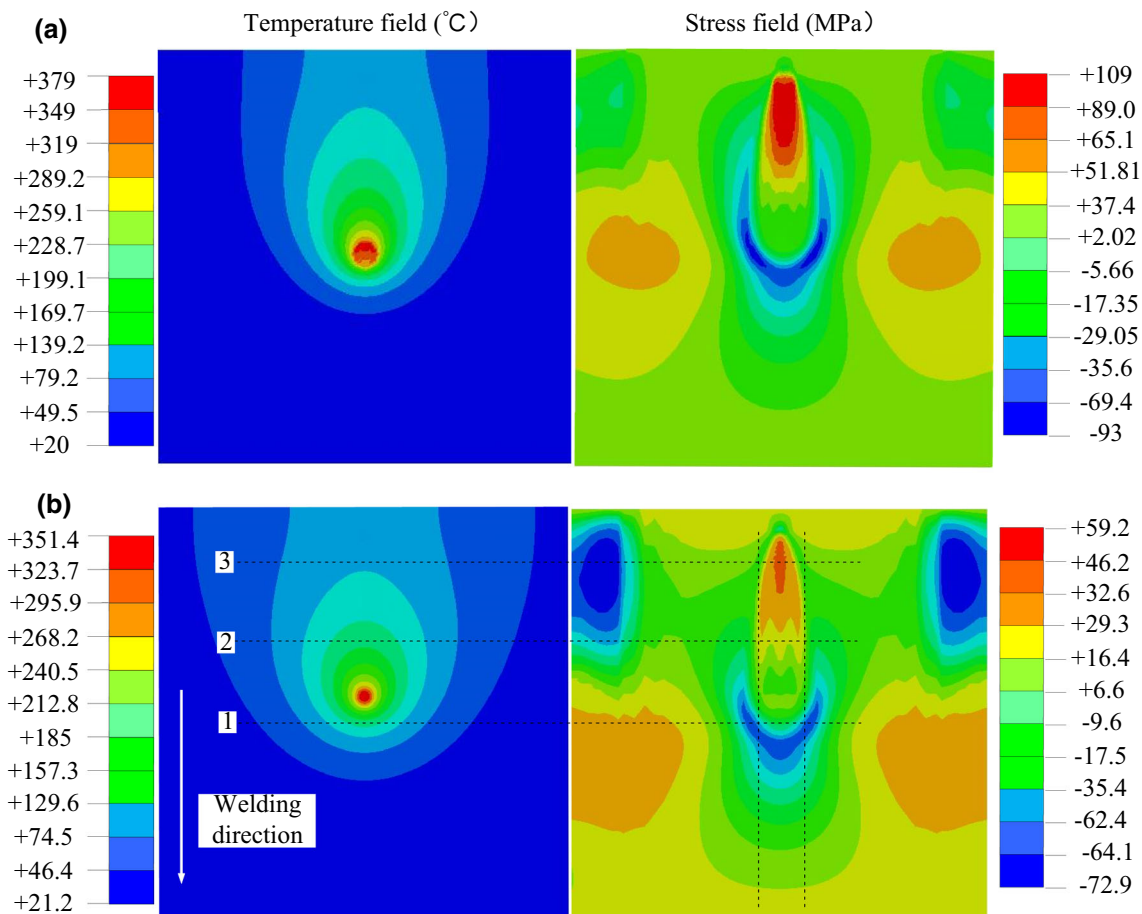
Fig. 11 Temperature and longitudinal stress fields with rotational velocity of 800 rpm by **a** FSW and **b** SSFSW
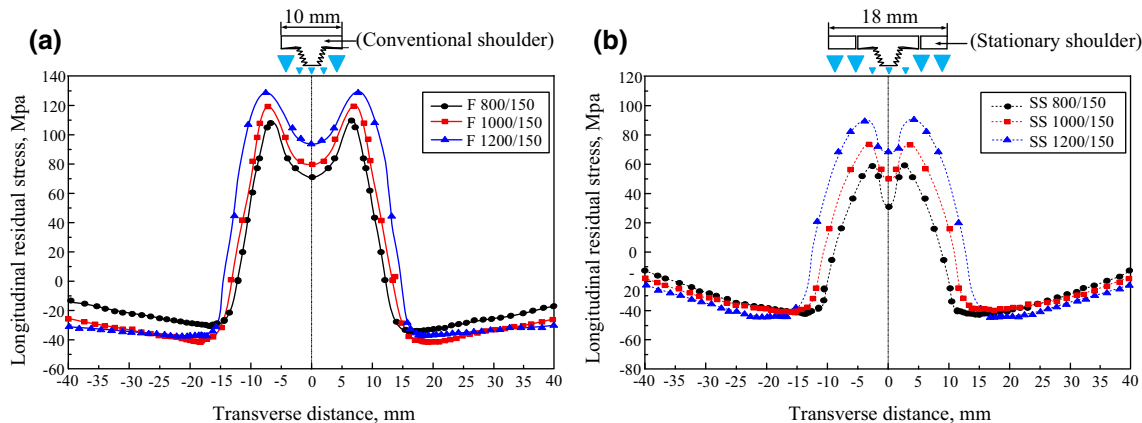

Fig. 12 Distributions of LRS perpendicular to the weld by **a** conventional FSW and **b** SSFSW

absorbs considerable frictional heat induced by the inside rotational tool. Moreover, an additional tensile strain is provided by the external stationary shoulder to the weld, which offsets the compressive strain caused in the heating stage. Thus, a relatively narrower TRS region and lower TRS for SSFSW are observed at the same rotational velocity compared with the conventional shoulder. The

maximum TRS at the rotational velocities of 800, 1000, and 1200 rpm by SSFSW are reduced to 59.3, 73.1, and 82.3 MPa, respectively. The relative decrement is approximately 45.9%.

The produced LRS along the plate thickness under two different processes with 800 mm/min rotational velocity are displayed in Fig. 13. For the conventional FSW, the
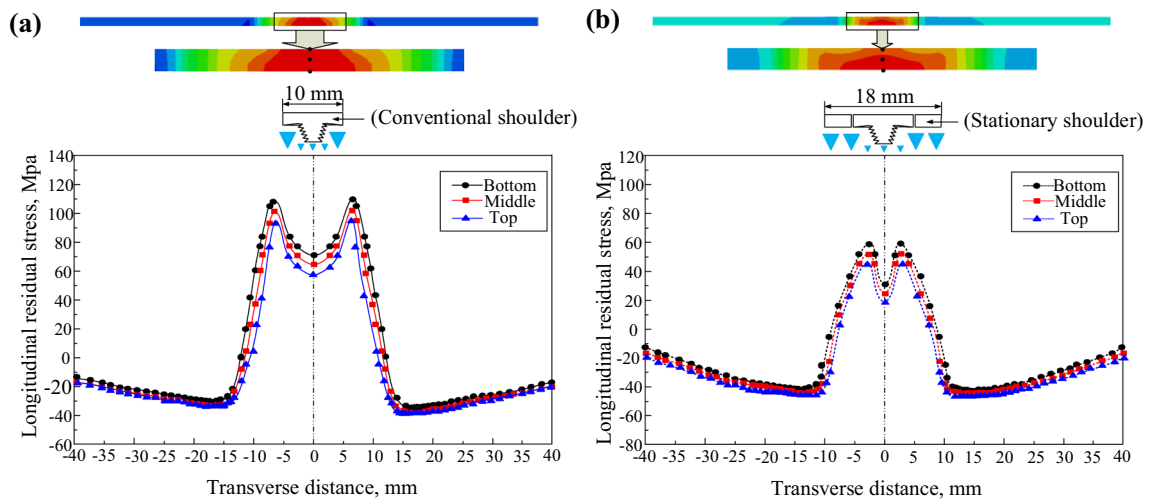
Fig. 13 LRS fields along the thickness and distribution curves perpendicular to the weld of **a** conventional FSW and **b** SSFSW
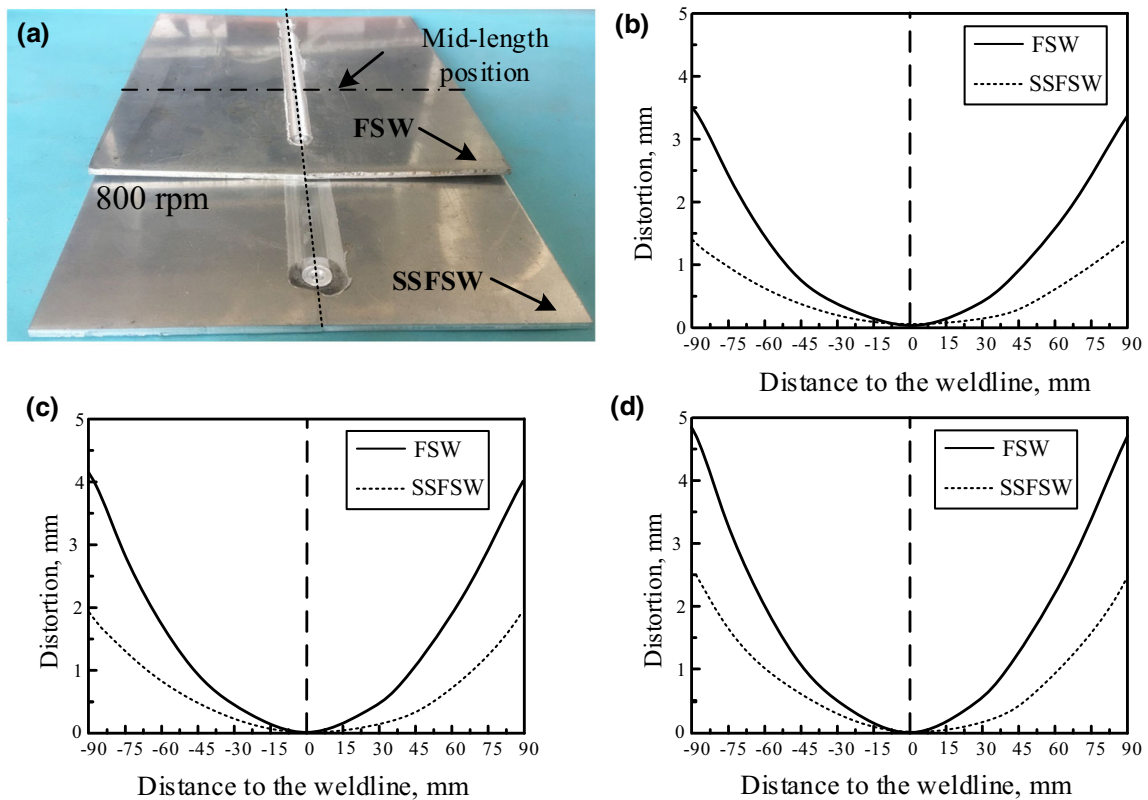

Fig. 14 **a** Distortion profiles of welded plates attained by experiment; comparisons of residual distortion distribution between conventional FSW and SSFSW at **b** 800 rpm, **c** 1000 rpm and **d** 1200 rpm

width of TRS region is approximately the SAZ width on the top surface and this width gradually increases with the increase in distance from the top surface. According to the previous research [26], the friction behavior can make the stress distributed non-uniformly through the plate thickness direction. In this study, the above-mentioned TRS width near the weld is decided by the reducing effect of TRS

along the plate thickness by the rotational shoulder, since the width of region with high temperature decreases with the increase in distance from the top surface of the plate (Fig. 8).

The LRS curves of three positions (top, middle, and bottom) are drawn in Fig. 13a and b. Although the LRS values varies, the tendency of three curves is generally in

good agreement. For the thin plate with the thickness less than 3.0 mm, Deng et al. [27] indicated that no difference in longitudinal stress between the top and bottom surfaces has been observed. However, the peak TRS at the bottom surface is relatively higher than the corresponding stress at the top surface in this study, which verifies that the reducing effect of TRS by the rotational shoulder gradually weakens with the increase in distance from the plate top surface. For the conventional FSW process, the peak TRS on the top surface is 91 MPa, the value by SSFSW is 42.3 MPa. The peak TRSes at the bottom surface under FSW and SSFSW processes are 109.8, and 59.3 MPa, respectively. This phenomenon on the reducing effect of TRS by the stationary shoulder results from the rolling effect of stationary shoulder.

Large elastic and plastic distortion of thin plate can be induced due to the high welding thermal input during welding. The pressing plates were not removed immediately after welding, so the thermal stress was restrained, and no distortion was developed. The clamps were removed when the entire plate reached the ambient temperature. Then, the welding distortion was produced. Figure 14a compares the experimental results of welding distortion for the conventional FSW and SSFSW when the rotational velocity is 800 rpm. On the basis of distortion profiles in Fig. 14a, the welding distortion is significant for the conventional FSW and not obvious for the SSFSW. Distortion is greatly reduced by the stationary shoulder. Residual distortion distributions in the mid-length position perpendicular to the weld for both the processes are shown in Fig. 14b, c and d. Residual distortion increases with the increase in rotational velocity. In addition, the distortion values of SSFSW are smaller than those of FSW under the same rotational velocity. The maximum distortions for conventional FSW are 3.5, 4.2, and 4.7 mm when the rotational velocities are 800, 1000, and 1200 rpm, respectively. For the SSFSW, the maximum distortions are 1.4, 1.9, and 2.5 mm, respectively. The high plunge force provided by the stationary shoulder plays a synchronous rolling role on the weld. This function can effectively prevent plastic distortion in the welding process. Furthermore, the stationary shoulder absorbs a portion of frictional heat, as discussed in Sect. 4.2, which is also beneficial to control the welding distortion of thin plate.

5 Conclusions

In this study, the stationary shoulder was utilized to control the welding residual stress and distortion of FSW butt joint. In addition, a thermo-elastic–plastic FEM was developed to predict the temperature and residual stress fields. Moreover, comparisons of temperature, stress and distortion between the conventional and stationary shoulder processes were achieved. On the basis of the experimental and simulation results, the following conclusions were drawn as follows:

1. Under the selected rotational velocities, defect-free joints were obtained. The widths of SZ and SAZ in the cross section of the joint increased with the increase in rotational velocity. The width of SAZ was greatly reduced by adding the stationary shoulder.

2. High local TRS was situated at the transition region between SZ and HAZ, which was mainly derived from the high temperature and mechanical force caused by the rotational shoulder. For the SSFSW, the stationary shoulder provided an additional tensile strain to the weld, which was beneficial in offsetting the compressive plastic strain and in controlling the residual stress. The peak TRS of the SSFSW was approximately 45.9% smaller than that of the conventional FSW.

3. Higher rotational velocity caused higher peak temperature of weld in both processes. The thermal gradient had a significant effect on the generation of welding distortion. The external stationary shoulder absorbed a mass of frictional heat and applied a synchronous rolling during welding. Therefore, the external stationary shoulder significantly eliminated distortion in FSW.

Compliance with Ethical Standards

Conflict of interest The authors declare that they have no conflict of interest.

References

1. Liu H J, Fujii H, Maeda M, and Nogi K, *J Mater Process Technol* **142** (2003) 692.
2. Simar A, Bréchet Y, Meester B D, Denquin A, and Pardoen T, *Mater Sci Eng A* **486** (2008) 85.
3. Aydin H, Durmuş A, Bayram A, and Sayaca T, *Trans Indian Inst Met* **65** (2012) 21.
4. Ma Z W, Jin Y Y, Ji S D, Meng X C, Ma L, and Li Q H, *J Mater Sci Technol* **35** (2019) 94.
5. Wang X H, and Wang K, *Mater Sci Eng A* **431** (2006) 114.
6. Dinaharan I, Murugan N, and Parameswaran S, *Trans Indian Inst Met* **65** (2012) 159.
7. Lombard H, Hattingh D G, Steuwer A, and James M N, *Mater Sci Eng A* **501** (2009) 119.
8. Long T, Tang W, and Reynolds A P, *Sci Technol Weld Join* **12** (2007) 311.
9. Riahi M, and Nazari H, *Int J Adv Manuf Technol* **55** (2011) 143.

10. Giorgi M D, Scialpi A, Panella F W, and Filippis L A C D, *J Mech Sci Technol* **23** (2009) 26.
11. Tufaro L N, Burgueno A, and Svoboda H G. *Soldagem Insp* **17** (2012) 327.
12. Ji S D, Yang Z P, Wen Q, Yue Y M, and Zhang L G, *High Temp Mater Process* **37** (2018) 397.
13. Kim Y G, Fujii H, Tsumura T, Komazaki T, and Nakata K, *Mater Sci Eng A* **415** (2006) 250.
14. Richter-Trummer V, Suzano E, Beltrão M, Roos A, and Santos J F D, *Mater Sci Eng A* **538** (2012) 81.
15. Jiang X, Wynne B P, and Martin J, *J Mater Sci Technol* **34** (2018) 198.
16. Russell M J, Blignault C, Horrex N L, and Wiesner C S, *Weld World* **52** (2008) 12.
17. Li Z W, Yue Y M, Ji S D, Chai P, and Zhou Z L, *Mater Des* **90** (2016) 238.
18. Sun T, Roy M J, Strong D, Withers P J, and Prangell P B, *J Mater Process Technol* **242** (2017) 92.
19. Li D X, Yang X Q, Cui L, He F Z, and Zhang X, *J Mater Process Technol* **222** (2015) 391.
20. Ji S D, Meng X C, Liu J G, Zhang L G, and Gao S S, *Mater Design* **62** (2014) 113.
21. Wang L, Davies C M, Wimpory R C, Xie L Y, and Nikbin K M, *Mater High Temp* **27** (2010) 167.
22. Cao X, and Jahazi M, *Mater Des* **30** (2009) 2033.
23. Wu C S, Zhang W B, Shi L, and Chen M A, *Trans Nonferrous Met Soc* **22** (2012) 1445.
24. Bachmann M, Carstensen J, Bergmann L, Dos Santos J F, Wu C S, and Rethmeier M, *Int J Adv Manuf Technol* **91** (2016) 1443.
25. Camilleri D, Micallef D, and Mollicone P, *J Therm Stresses* **38** (2015) 485.
26. Cozzolino L D, Coules H E, Colegrove P A, and Wen S, *J Mater Process Technol* **247** (2017) 243.
27. Deng D, and Murakawa H, *Comput Mater Sci* **43** (2008) 681.